Inorganic Chemistry

Article

pubs.acs.org/IC

Structure and Spectroscopic Properties of Nickel Benzazolate Complexes with Hydrotris(pyrazolyl)borate Ligand

Luisa López-Banet,[†] M. Dolores Santana,*[,†] María José Piernas,[†] Gabriel García,[†] Javier Cerezo,[‡] Alberto Requena,[‡] José Zúñiga,*[,‡] José Pérez,[§] and Luís García[§]

[†]Departamento de Química Inorgánica, Universidad de Murcia, E-30071 Murcia, Spain

[‡]Departamento de Química Física, Universidad de Murcia, E-30071 Murcia, Spain

[§]Departamento de Ingeniería Minera, Geológica y Cartográfica, Área de Química Inorgánica, Universidad Politécnica de Cartagena, E-30203 Cartagena, Spain

Supporting Information

ABSTRACT: The reaction of benzazole ligands 2-(2′-hydroxylphenyl)-benzimidazole (Hpbm), 2-(2′-hydroxylphenyl)benzoxazole (Hpbx), and 2-(2′-hydroxylphenyl)benzothiazole (Hpbt), with $[Ni(Tp^*)(\mu\text{-}OH)]_2$ (Tp^* = hydrotris(3,5-dimethylpyrazolyl)borate), leads to pentacoordinate nickel complexes $[Ni(Tp^*)(pbz)]$ (pbz = pbm (**1**), pbx (**2**), pbt (**3**)). The structures of **1**, **2**, and **3** were determined by X-ray crystallography. The pentacoordinate nickel complexes have distorted trigonal bipyramidal geometries with Addison's τ parameter values of 0.63, 0.73, and 0.61 for **1**, **2** and **3**, respectively. The benzazolates are bonded in an η^2(N,O) fashion to the nickel atoms. DFT calculations are carried out to optimize the structures of the three complexes giving a good agreement with the X-ray structures. The ^{1}H NMR spectra of complexes **1**−**3** exhibit sharp isotropically shifted signals. The complete assignment of these signals required an application of two-dimensional $\{^1H-^1H\}$-COSY techniques. The experimental absorption spectra of the three complexes in chloroform solution each show an intense absorption band in the ultraviolet region ca. 240 nm, followed by three less intense bands, the first two at ∼295 and ∼340 nm, and the last more disperse one, at wavelengths between 360 and 410 nm. The absorption spectra are simulated by TD-DFT and reproduce the main features of the experimental spectra well. The analysis of the electronic transitions by inspection of the frontier molecular orbitals and also the natural transition orbitals allowed us to characterize and assign the observed bands properly. The three complexes are moderately blue luminescent at room temperature, both in the solid state and in solution. Emission spectra at room temperature display broad structureless bands in chloroform solution at 460, 482, and 512 nm for complexes **1**, **2** and **3**, respectively, and structured emission in solid state with λ_{max} values of 473, 486, and 516 nm. Complexes containing different donor atoms in the benzazole ligand are furthermore observed to give different luminescence responses in the presence of Zn(II), Cd(II), Hg(II), and Cu(II).

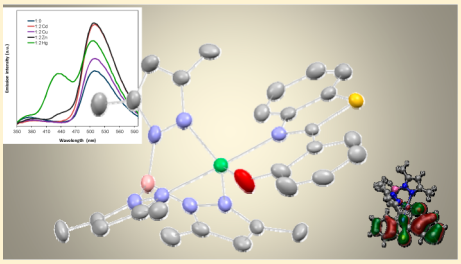

INTRODUCTION

Coordination compounds containing fluorescent ligands have attracted a vast amount of attention due to their applications, especially in modern electronics, as materials for producing light-emitting diodes (OLEDs).[1] 2-(2′-Hydroxylphenyl)-benzazoles (Hpbz) are in this context chemically and photochemically stable compounds whose metal complexes are of great interest for the OLED technology, as indicated by several patents.[2−5] Transition metal coordination compounds containing benzimidazolic ligands have also drawn attention from several research groups, since benzimidazoles and benzoxazoles display important properties that span from luminescence[6−9] to biocidal activities.[10−14] Benzazole ligands have an electronic system similar to that of 8-hydroxyquinoline, with ligands containing at least one hydroxyl group, a coordination nitrogen atom, and a delocalized π-system. Benzazoles, in particular, whose skeleton is depicted in Scheme 1, have one acidic proton (—OH) in close proximity to a basic center (—N═), and show high intensity of fluorescence emission and large Stokes shift in ESIPT (excited state intramolecular proton transfer).[15,16]

A considerable number of experimental and theoretical studies have been conducted on representative ESIPT molecules such as salicylidene anilines, quinolines, and also 2-

Scheme 1

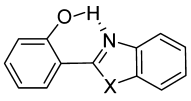

X	benzazole	Hpbz
NH	2-(2'-hydroxylphenyl)benzimidazole	Hpbm
O	2-(2'-hydroxylphenyl)benzoxazole	Hpbx
S	2-(2'-hydroxylphenyl)benzothiazole	Hpbt

Received: January 22, 2014
Published: May 21, 2014

 © 2014 American Chemical Society dx.doi.org/10.1021/ic5001655 | Inorg. Chem. 2014, 53, 5502−5514

(2′-hydroxylphenyl)benzazole derivatives,[17,18] and attract much interest for use in various optical applications.[19,20] Among ESIPT fluorophores, 2-(2′-hydroxylphenyl)benzazoles (Scheme 1) represent an interesting family of ligands which can bind metal ions (e.g., Be, Zn, Cd, Ni, Co, Pd).[21−24] Homoleptic M(pbz)-type complexes provide, however, relatively limited possibilities for tuning their photophysical properties, which are essentially determined by their molecular structure and molecular packing characteristics. Well-defined heteroleptic molecular complexes supported by benzazole ligands with novel core structures and controllable photoluminescence features become then a very promising option, and the development of new routes to synthesize them constitutes a big challenge for chemists.

Luminescent d^8 transition metal complexes are currently, in addition, under intense investigation for both theoretical purposes[25] and their applications.[26] Metals such as Pt(II)[27] and Pd(II)[28] occupy a notable position despite the fact that the majority of the systems containing palladium, in particular, emit only at low temperatures.[29] For nickel only a few species have been reported,[30] and to the best of our knowledge, the theoretical studies performed are scarce.[31] The spectroscopic properties of nickel derivatives can be effectively tuned by the appropriate choice of ancillary ligands and ligand substituents. It is important to notice that the electronic properties of substituents in conjugated systems very often shift HOMO and LUMO energies in the same direction, poorly influencing the HOMO−LUMO energy gap,[30e] so the admixture of metal and ligand orbitals results in an additional and somewhat critical parameter for the design of blue light emitters.[30c]

Apart from their interest in several applied fields, the synthetic value of nickel group di-μ-hydroxo-complexes is a subject of continuous study.[32] We have contributed to this area by exploiting the usefulness of dinuclear hydroxo-complexes of nickel, some of them with a macrocyclic backbone,[33] in the preparation of a wide variety of new compounds by means of a simple acid−base reaction.[34] In this context, and in line with our interest in studying the photophysical properties of pentacoordinate complexes of nickel(II), in this work we synthesize benzazolate complexes containing the fragment "Ni(Tp*)" (Tp* = hydrotris(3,5-dimethylpyrazolyl)borate). Hydrotris(3,5-dimethylpyrazolyl)borate was selected as ancillary ligand for nickel(II) due to the great interest that tris(pyrazolylborate) compounds have. In particular, they act as monoanionic tripodal ligands and leave at least one coordination site available for another donor group which is especially suitable to develop homogeneous catalysis or metalloenzyme active sites models or to synthesize polynuclear complexes.[35,36]

In this Article, we describe the syntheses, crystal structures, and spectroscopic absorption properties of pentacoordinate Ni(II) complexes of aromatic N,O-chelate ligands, along with density functional theory (DFT) calculations conducted to support them. In addition, we characterize the luminescence properties of the complexes in solution and the solid state, and the fluorescent responses observed in the presence of cations of physiological and toxicological importance such as Zn(II), Cd(II), Hg(II), and Cu(II).

RESULTS AND DISCUSSION

Synthesis and Crystal Structures. In previous works[37] we reported the preparation of several mono- and dinuclear complexes containing Tp* backbones combined with several phosphate ligands. The hydroxo-complex[38] $[Ni(Tp^*)(\mu\text{-}OH)]_2$ has been employed as a convenient precursor in the preparation of a wide variety of complexes, by means of acid−base reactions. Thus, complexes **1**−**3** ([Ni(Tp*)(pbz)] (pbz = pbm, pbx, pbt) were synthesized by reaction between the hydroxo-complex $[Ni(Tp^*)(\mu\text{-}OH)]_2$ and the corresponding benzazole ligand [Hpbm = 2-(2′-hydroxylphenyl)enzimidazole, Hpbx = 2-(2′-hydroxylphenyl)benzoxazole, and Hpbt = 2-(2′-hydroxylphenyl)benzothiazole], in chloroform at room temperature, as depicted in Scheme 2. Compounds **1**−**3** were

Scheme 2. Synthesis of Complexes 1−3 and Atom Numbering

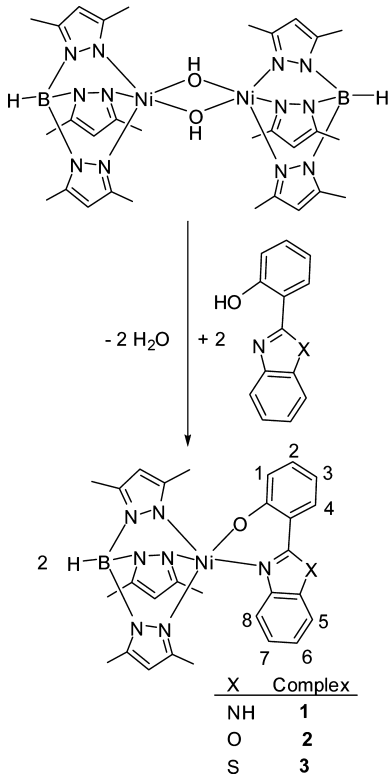

characterized by mass spectrometry, IR, and ^{1}H NMR spectroscopies, and absorption and fluorescence measurements. Besides, crystal structures were obtained for all complexes.

The molecular structures of complexes **1**−**3** have been elucidated by single-crystal X-ray diffraction analyses. Perspective drawings are shown in Figures 1−3, and selected interatomic parameters are given in Table 1. Complexes **1**−**3** are monomers with five-coordinate nickel atoms. The coordination geometry around nickel atoms is a distorted trigonal bipyramid, as ascertained by the Addison's τ parameter[39] connecting regular trigonal bipyramidal (τ = 1) and regular square-base pyramidal (τ = 0) structures, which gives values of 0.63, 0.73, and 0.61 for complexes **1**, **2**, and **3**, respectively. The nitrogen atoms of the Tp* ligand arms hold one apical position, N5, and two adjacent equatorial positions, N1 and N3, whereas the remaining equatorial and apical positions are occupied, respectively, by O1 and N7 atoms of the benzazolate ligand. The equatorial plane is thus formed by atoms N1, N3, and O1. The six-membered "Ni1−N7−C22−C21−C16−O1" chelate rings are nonplanar, while the individual phenyl and benzazolate rings are planar. The planes defined by the "Ni1−N7−C22" rings and O1−C16···C21

dx.doi.org/10.1021/ic5001655 | Inorg. Chem. 2014, 53, 5502−5514

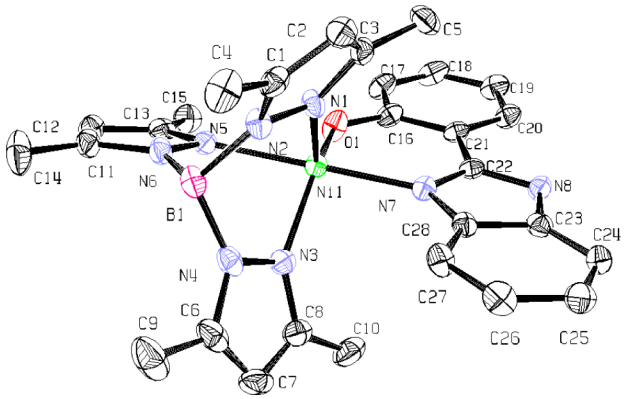

Figure 1. ORTEP drawing of complex **1** (ellipsoids at 50% probability level) with atom-labeling scheme.

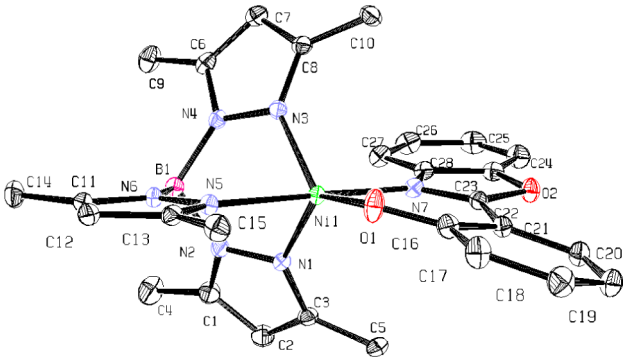

Figure 2. ORTEP drawing of complex **2** (ellipsoids at 50% probability level) with atom-labeling scheme.

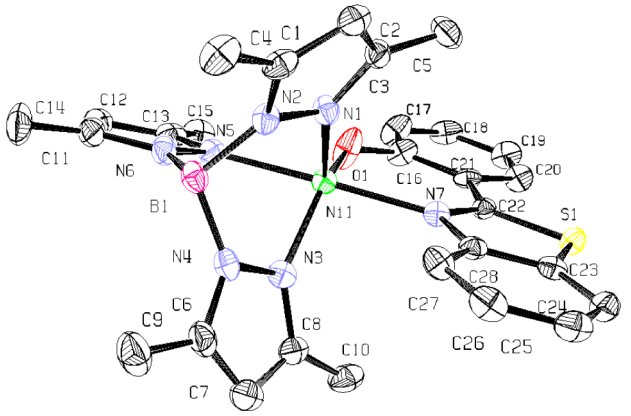

Figure 3. ORTEP drawing of complex **3** (ellipsoids at 50% probability level) with atom-labeling scheme.

phenyl rings form angles of 5.22° in **1**, 11.24° in **2**, and 1.80° in **3**. The benzazolates are bonded in an η^2(N,O) fashion to the nickel atoms. The Ni−O bond distances are 1.9228, 1.9461, and 1.9114 Å for complexes **1**, **2**, and **3**, respectively, shorter than those observed in the mixed-ligand complex $[(Tp^{CO^2Me,Me})Ni(Gly)(H_2O)]ClO_4$,[40] whereas the Ni−$N_{pbz}$ bond distances are a little longer, 2.0495, 2.0594, and 2.091 Å for **1**, **2**, and **3**, respectively. The N−Ni−O "bite" angles of the chelating benzazolates are 88.91° in **1**, 87.77° in **2**, and 89.07° in **3**, with no proper comparisons made since complexes containing the moiety Ni(Tp*) and similar chelate ligands have not been reported so far.

Geometry Optimization. The structures of complexes **1**−**3** were optimized *in vacuo* using the BP86 density functional in combination with the LANL2TZ+ basis for Ni and the cc-pVDZ basis for the rest of the atoms and starting from the corresponding X-ray structures. The optimized bond lengths and angles of the nickel coordination geometries are given in Table 1 along with the experimental ones. We also include in this table the root-mean-squares deviations (RMSD) of the lengths and angles of the distorted trigonal bipyramids, and the RMSD of all the lengths and angles of the complexes. As a whole, the electronic structure calculations provide a reasonably good description of the geometries of the three complexes within the usual levels of accuracy provided by the DFT methods.[41] Going into details, we see that the RMSD values for the nickel bond lengths are of the order of 0.020 Å, with the calculated lengths slightly overestimating systematically the observed X-ray values. The RMSDs for the nickel bond angles are, respectively, 1.07°, 2.73°, and 1.74° for complexes **1**, **2**, and **3**. In this case, the largest differences with the X-ray structures occur in the two equatorial plane angles O(1)−Ni(1)−N(1) and O(1)−Ni(1)−N(3) of complexes **2** and **3**, with deviations of about 5° for complex **2** and 3° for complex **3**. The τ parameters calculated for the optimized structures, also included in Table 1, are somewhat lower than those corresponding to the X-ray structures, which indicate that the optimized structures are somewhat more shifted toward the regular square base pyramid limit. These angular deviations could be due to crystal packing effects, which were not considered in the electronic structure calculations, or to limitations in the level of theory employed. Nevertheless, the RMSDs for all the bond lengths and all the bond angles of the complexes are smaller than those obtained for the nickel coordination geometries, especially for the angles, with averaged values for the whole geometries of 0.019 Å for the lengths and 0.88° for the angles. This accuracy is, in principle, quite satisfactory for the confident use of the optimized geometries in the theoretical simulations of the electronic absorption spectra of the complexes.

^{1}H NMR Spectra. The ^{1}H NMR spectra of the three complexes exhibit sharp isotropically shifted signals ranging from 85 ppm (downfield) to −10 ppm (upfield), in chloroform solution. The spectra show the resonance line pattern observed for the Tp* ligand complexes, assigned on the basis of previous studies of nickel in accordance with the observed properties of protons of the pyrazolyl ring in other Ni($Tp^{R1,R2}$) complexes.[37] A representative proton NMR spectrum for complex **3** is shown in Figure 4, and similar spectra of complexes **1** and **2** are given in the Supporting Information (Figures S1 and S2). The ^{1}H NMR spectra of the three compounds show two sets of resonances for the three pyrazolyl rings as is to be expected from their X-ray structures described above. Thus, for example, in complex **3** (Figure 4) one of these rings gives rise to three singlets at about δ = −7.77, −2.96, and 68.01 ppm, in a 3:3:1 ratio, corresponding to the 3-Me_{ax}, 5-Me_{ax}, and 4-H_{ax} pyrazolyl protons, respectively (see Scheme 2 for the numbering scheme). Another set of resonances due to the two equatorial rings show three singlets at about δ = −9.96, 1.45, and 62.71 ppm, in a 6:6:2 ratio, corresponding to the 3-Me_{eq}, 5-Me_{eq}, and 4-H_{eq} pyrazolyl protons, respectively.

The complete assignment of all isotropically shifted signals required an application of two-dimensional ^{1}H NMR techniques. A portion of the {^{1}H−^{1}H}-COSY spectrum of complex **3** recorded at 20 °C is shown in Supporting

dx.doi.org/10.1021/ic5001655 | Inorg. Chem. 2014, 53, 5502−5514

Table 1. Selected Bond Lengths (Å) and Bond Angles (deg) for Complexes 1, 2, and 3

	complex **1**		complex **2**		complex **3**	
param	expt	optimized	expt	optimized	expt	optimized
Ni(1)−O(1)	1.9228(13)	1.972	1.9462(15)	1.975	1.9114(19)	1.954
Ni(1)−N(1)	2.0139(16)	2.031	2.0249(16)	2.047	2.006(2)	2.022
Ni(1)−N(3)	2.0279(17)	2.049	2.0176(16)	2.033	2.022(2)	2.042
Ni(1)−N(7)	2.0495(17)	2.076	2.0594(16)	2.081	2.091(2)	2.135
Ni(1)−N(5)	2.1293(18)	2.156	2.1105(16)	2.143	2.117(2)	2.159
RMSD (lengths)		0.02		0.018		0.025
O(1)−Ni(1)−N(1)	122.67(7)	123.28	135.24(7)	140.38	122.87(10)	119.76
O(1)−Ni(1)−N(3)	142.12(6)	142.86	131.98(7)	126.01	142.32(10)	145.51
N(1)−Ni(1)−N(3)	94.89(7)	93.68	92.79(6)	93.35	94.51(9)	94.32
O(1)−Ni(1)−N(7)	88.91(8)	87.60	87.76(6)	87.24	89.07(9)	88.14
N(1)−Ni(1)−N(7)	93.00(7)	94.35	90.78(6)	93.06	92.93(8)	95.22
N(3)−Ni(1)−N(7)	94.30(7)	93.62	92.66(6)	93.39	93.88(8)	94.19
O(1)−Ni(1)−N(5)	91.47(8)	92.57	93.32(6)	93.30	91.24(9)	91.44
N(1)−Ni(1)−N(5)	86.74(7)	87.35	87.96(6)	85.57	87.93(9)	87.69
N(3)−Ni(1)−N(5)	85.44(7)	84.95	87.14(6)	87.52	85.11(9)	84.40
N(7)−Ni(1)−N(5)	179.62(7)	177.84	178.71(6)	178.40	178.73(9)	176.86
RMSD (angles)		1.07		2.73		1.74
τ	0.63	0.58	0.72	0.63	0.61	0.52
RMSD (all lengths)		0.019		0.016		0.022
RMSD (all angles)		0.67		1.12		0.86

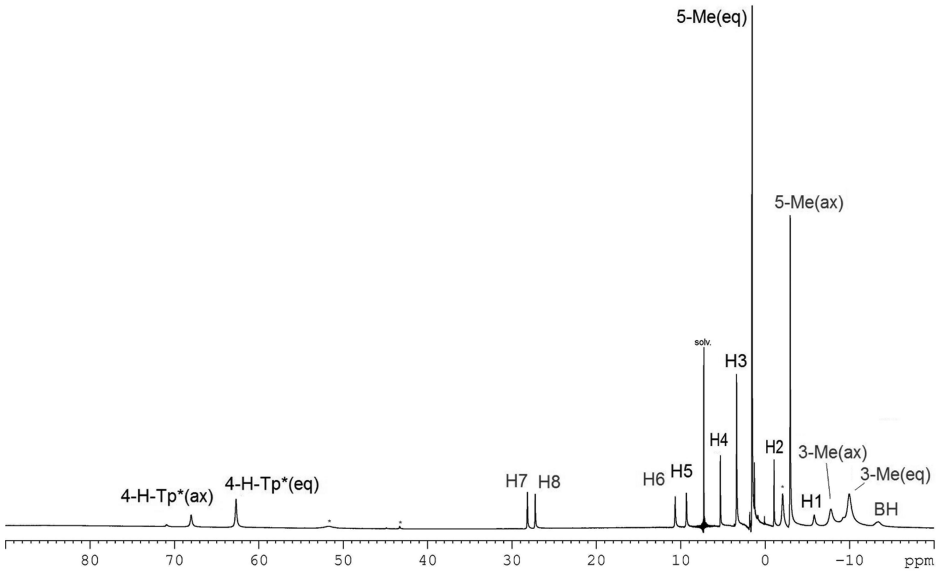

Figure 4. ^{1}H NMR spectrum of **3** (in $CDCl_3$ solution at room temperature, r.t.).

Information Figure S3 where cross signals between the 28.17, 27.25, 10.66, and 9.33 ppm resonances are observed. These signals can be assigned to H_7, H_8, H_6, and H_5 protons, respectively. COSY spectrum of **3** also shows cross signals between resonances at 5.30, 3.39, −1.05, and −5.81 ppm which are assigned to H_4, H_3, H_2, and H_1 protons, respectively. The alternating downfield, upfield pattern in the arylphenolate proton shifts reflects a hyperfine contact shifting because of electron spin delocalization onto the arylphenolate by a π-polarization pathway.[42] The protons of benzothiazole ring display a nearly constant downfield shift indicative of a second mechanism, such as direct spin delocalization through σ bonds, a behavior which has been similarly observed previously.[43]

Electronic Absorption Spectra. The experimental and calculated electronic absorption spectra of complexes **1**, **2**, and **3** in $CHCl_3$ solution are shown in Figures 5−7. As observed, all complexes have an intense absorption band in the ultraviolet region ca. 240 nm, with an extinction coefficient ε between 17 000 and 27 000 dm^3 mol^{-1} cm^{-1}, followed by three less intense bands, the first two at ∼295 and ∼340 nm, with ε of ∼15 000 and ∼8000 dm^3 mol^{-1} cm^{-1}, respectively, and the last more disperse one, at wavelengths between 360 and 410 nm. The calculated spectra reproduce reasonably well the observed bands despite being blue-shifted by about 30 nm. Accordingly, they are expected to be of help in the assignment of the experimental spectra. We should notice that blue-shifts of electronic spectra when simulated using the CAM-B3LYP density functional have been previously reported in recent applications to conjugated organic molecules[44] and transition metal complexes.[45]

In the calculated spectra shown in Figures 5−7, we have depicted the allowed transitions by vertical lines, and labeled

dx.doi.org/10.1021/ic5001655 | Inorg. Chem. 2014, 53, 5502−5514

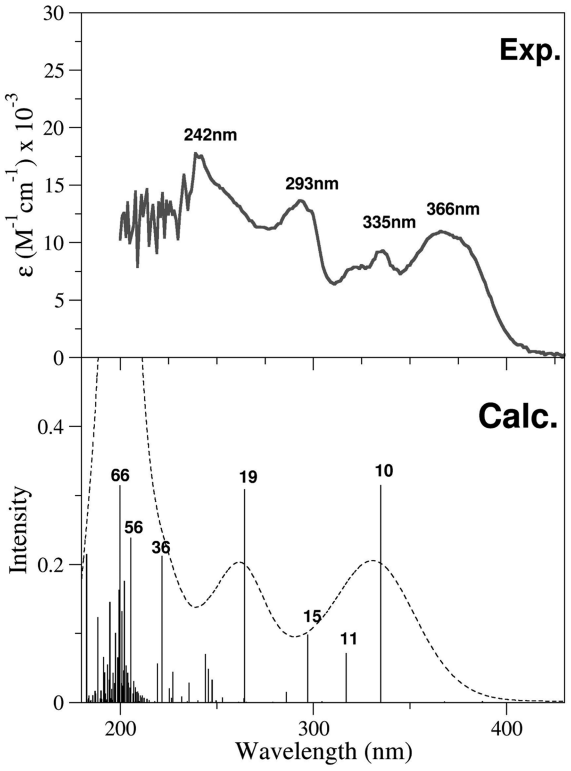

Figure 5. UV−vis absorption spectra of complex **1** measured (top panel) and calculated using the TD-CAM-B3LYP method (bottom panel), in $CHCl_3$ solution; vertical lines in calculated spectra indicate excited states and their corresponding oscillator strengths.

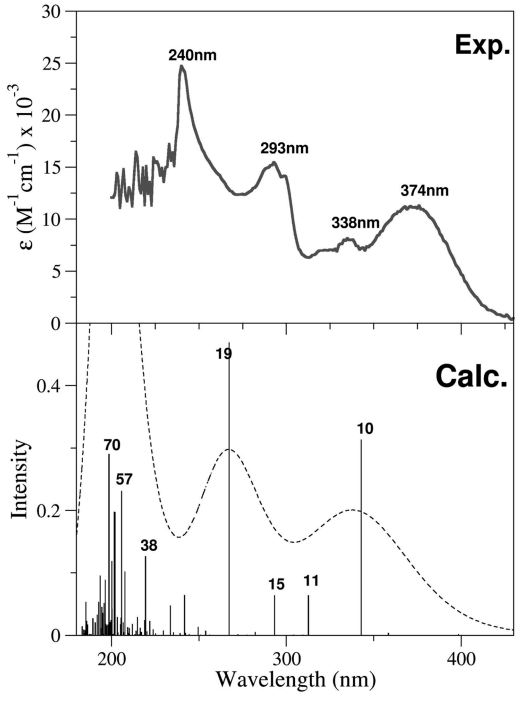

Figure 6. UV−vis absorption spectra of complex **2** measured (top panel) and calculated using the TD-CAM-B3LYP method (bottom panel), in $CHCl_3$ solution; vertical lines in calculated spectra indicate excited states and their corresponding oscillator strengths.

the most intense ones with the number of the excited state reached. To study the nature of the electronic transitions we

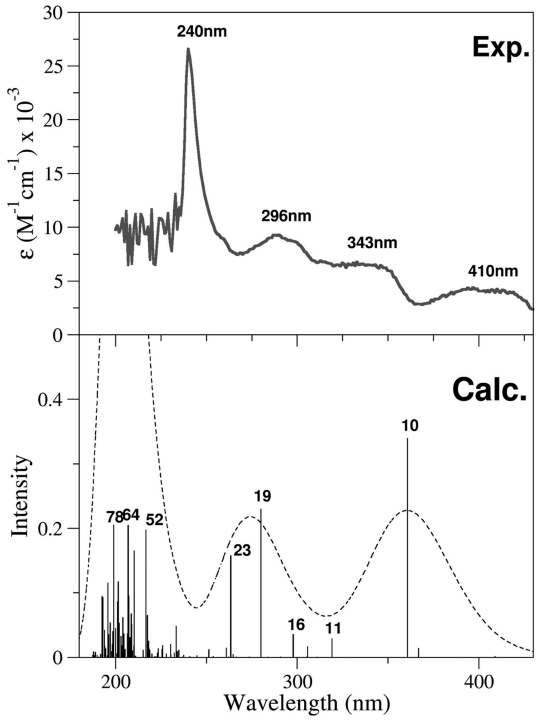

Figure 7. UV−vis absorption spectra of complex **3** measured (top panel) and calculated using the TD-CAM-B3LYP method (bottom panel), in $CHCl_3$ solution; vertical lines in calculated spectra indicate excited states and their corresponding oscillator strengths.

have used the canonic molecular orbitals MO, and also the natural transition orbitals NTO which describe best the electronic transitions as only one orbital excitations from the donor (hole) to the acceptor (electron) orbitals and therefore facilitate the qualitative assignment of the spectroscopic bands. Since all the electronic states are triplets, the α-spin and β-spin densities have to be analyzed separately, a fact that can be in turn conveniently used to grasp whether charge displacements in the electronic transitions occur from or toward the metal. Effectively, according to the crystal field theory, the unpaired α electrons occupy the metal orbitals, so it is expected that transitions with a higher α-spin contribution will undergo, with a certain charge transfer starting from the metal, transitions with a higher β-spin contribution proceed with charge transfer toward the metal, and those with similar α- and β-spin contributions occur with no significant participation of the metal.

The characteristics of the most important electronic transitions of the complexes and their assignments to the experimental bands are given in Tables 2−4. In Figure 8 and Supporting Information Figures S4 and S5 we show as well the ground-state molecular orbital energy diagrams for the most important transitions, with the MO electronic density contours superposed on them in order to reinforce the interpretation of the transitions. Regarding the MO diagrams (Figure 8), it is worth noticing that, according to the unrestricted scheme, the α- and β-spin orbitals are computed separately; however, both the MO energy and shape are almost identical for orbitals which are predominantly ligand-centered, such as the HOMO and LUMO orbital over the pbm ligand, while for metal centered orbitals electron unpairing differentiates α- and β-spin orbitals, such as in the case of the L + 1(β) orbital that accommodates an unpaired electron and misses the α

dx.doi.org/10.1021/ic5001655 | Inorg. Chem. 2014, 53, 5502−5514

Table 2. The Most Important Spin-Allowed Triplet−Triplet Electronic Transitions of Complex 1 Calculated Using the TD-CAM-B3LYP Method in $CHCl_3$ Solution and the Assignments to the Experimental Absorption Bands

state	λ_{calc} (nm)	contributions	character[a]	λ_{exp} (nm)
10	335	H(β) → L(β)	ILMMCT: π(pbm) → π^*(pbm)	366
		H(α) → L(α)		
11	317	H(β) → L + 1(β)	ILMMCT: π(pbm) → π^*(pbm)	335
15	297	H(β) → L + 1(β)	LMCT: π(pbm) → Ni	
19	264	H − 2(α) → L(α)	ILCT: π(pbm) → π^*(pbm)	293
		H − 1(β) → L(β)		
36	222	H(β) → L + 3(β)	ILCT: π (pbm) → σ^*(pbm)	242
56	205	H − 5(β) → L + 2(β)	LMCT	
66	200	H(β) → L + 4(β)	LL′CT: pbm → Tp*	

[a]ILMMCT, intraligand metal modified charge transfer transition; LMCT, ligand to metal charge transfer transition; ILCT, intraligand charge transfer transition; LL′CT, ligand to ligand charge transfer transition.

Table 3. The Most Important Spin-Allowed Triplet−Triplet Electronic Transitions of Complex 2 Calculated Using the TD-CAM-B3LYP Method in $CHCl_3$ Solution and the Assignments to the Experimental Absorption Bands

state	λ_{calc} (nm)	contributions	character[a]	λ_{exp} (nm)
10	343	H(β) → L(β)	ILMMCT: π(pbx) → π^*(pbx)	374
		H(α) → L(α)		
11	313	H(β) → L + 1(β)	LMCT: π(pbx) → Ni	338
15	293	H(β) → L + 1(β)	LMCT: π(pbx) → Ni	
19	267	H − 2(α) → L(α)	ILCT: π(pbx) → π^*(pbx)	293
		H − 2(β) → L(β)		
38	219	H(β) → L + 3(β)	L′LCT: Tp* → pbx	240
57	206	H − 4(β) → L + 2(β)	L′MCT: Tp* → Ni	
70	199	H − 5(β) → L + 4(β)	IL′CT	

[a]ILMMCT, intraligand metal modified charge transfer transition; LMCT, ligand to metal charge transfer transition; ILCT, intraligand charge transfer transition; L′LCT, ligand to ligand charge transfer transition.

counterpart in the energy diagram. In addition, Figure 9 contains the NTO isosurfaces of some selected excited states of complex **1**. The NTO plots of all the excited states essentially involved in the absorption spectra are given in the Supporting Information.

For complex **1**, the lowest energy transition allowed is the one that takes place to the excited electronic state 10 and is easily identified as the HOMO to LUMO (H → L) transition. The MO contours for this transition show that the electronic densities concentrate in the pbm ligand (see Figure 8). The H(β) → L(β) contribution is moreover a bit higher than the H(α) → L(α) contribution, what anticipates a certain participation of the metal in the transition as commented above. The corresponding NTO isosurfaces shown in Figure 9 effectively confirm that the Ni atom receives a small amount of charge from the pbm ligand. Accordingly, the lowest energy H → L transition can be identified as a $\pi \rightarrow \pi^*$ transition within

Table 4. The Most Important Spin-Allowed Triplet−Triplet Electronic Transitions of Complex3 Calculated Using the TD-CAM-B3LYP Method in $CHCl_3$ Solution and the Assignments to the Experimental Absorption Bands

state	λ_{calc} (nm)	contributions	character[a]	λ_{exp} (nm)
10	361	H(β) → L(β)	ILMMCT: π(pbt) → π^*(pbt)	410
		H(α) → L(α)		
11	319	H(β) → L + 1(β)	LMCT: π(pbt) → Ni	343
16	298	H(β) → L + 1(β)	LMCT: π(pbt) → Ni	
19	280	H − 2(α) → L(α)	ILCT: π(pbt) → π^*(pbt)	296
		H − 2(β) → L(β)		
23	263	H − 4(α) → L(α)	ILCT: π(pbt) → π^*(pbt)	
		H − 4(β) → L(β)		
52	217	H(β) → L + 5(β)	L′MCT: Tp* → Ni	240
64	207	H(β) → L + 7(β)	LMCT	
78	207	H(α) → L + 2(α)	MLCT	

[a]ILMMCT, intraligand metal modified charge transfer transition; LMCT, ligand to metal charge transfer transition; ILCT, intraligand charge transfer transition; MLCT, metal to ligand transfer transition.

the benzimidazolate ligand slightly perturbed by the metal coordination, that is, a ILMMCT transition which gives rise to the absorption band of the complex observed at 366 nm.

The next two most intense transitions appearing in the simulated spectra of complex **1** are those to the excited states 11 and 15 (see Table 2). The MO analysis identifies now both transitions as H → L + 1, with the β-spin component being noticeably higher than the α-spin component. This indicates that an important amount of charge is, in principle, transferred to the metal, as clearly observed in the MO contours for these transitions shown in Figure 9. Since the two transitions have the same MO contributions, we have to resort in this case to the NTO isosurfaces to differentiate them. As observed in Figure 9, the transition to the excited state 11 almost exclusively affects the pbm ligand, with a minor withdrawal of charge by the metal, so it is therefore another ILMMCT transition. The transition to state 15 has, however, quite a different nature. Here we do indeed see a substantial displacement of charge from the pbm ligand to the Ni atom, as observed both in the corresponding NTO isosurface (Figure 9) and in the L + 1(β) orbital (Figure 8). This ligand-to-metal charge-transfer (LMCT) transition is exclusive therefore to the complex and results in the small absorption band that it exhibits at 335 nm presumably reinforced with ILMMCT transition to state 11.

The following transition in complex **1** takes place to the excited state 19 and is composed essentially of components H − 2(α) → L(α) and H − 1(β) → L(β) with similar weights (see Supporting Information Figure S4). No significant participation of the metal in these transitions is therefore expected, as evidenced by the NTO isosurfaces displayed in Figure 9 which show that the electronic densities spread over the pbm ligand. This is therefore an intraligand $\pi \rightarrow \pi^*$ charge-transfer (ILCT) transition that gives rise to the absorption band of the complex appearing around 293 nm.

dx.doi.org/10.1021/ic5001655 | Inorg. Chem. 2014, 53, 5502−5514

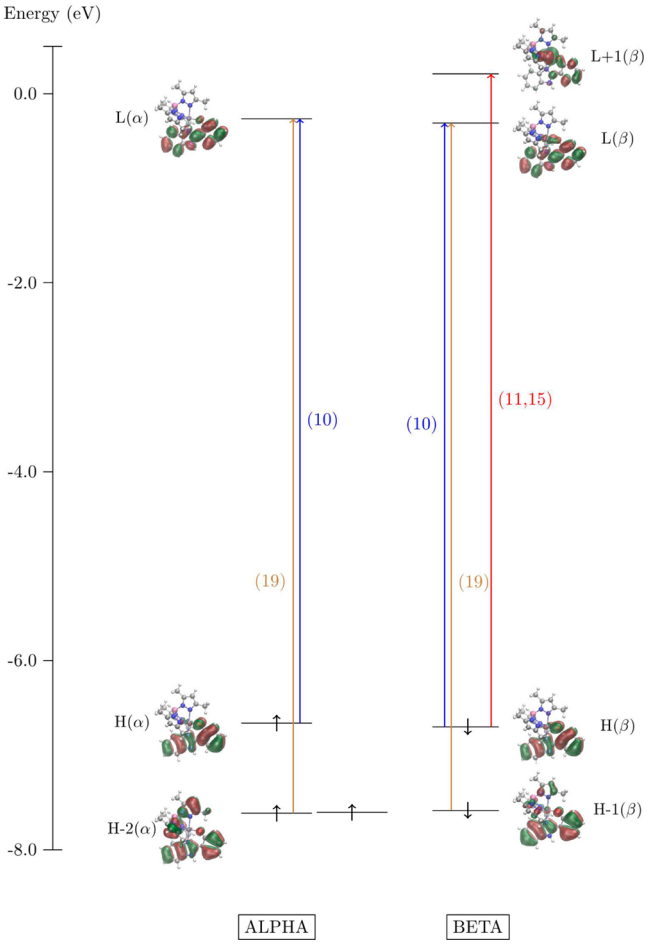

Figure 8. Ground-state molecular orbital energy diagram for the most important transitions of complex **1** along with the corresponding MO plots, calculated using the TD-CAM-B3LYP method in $CHCl_3$ solution.

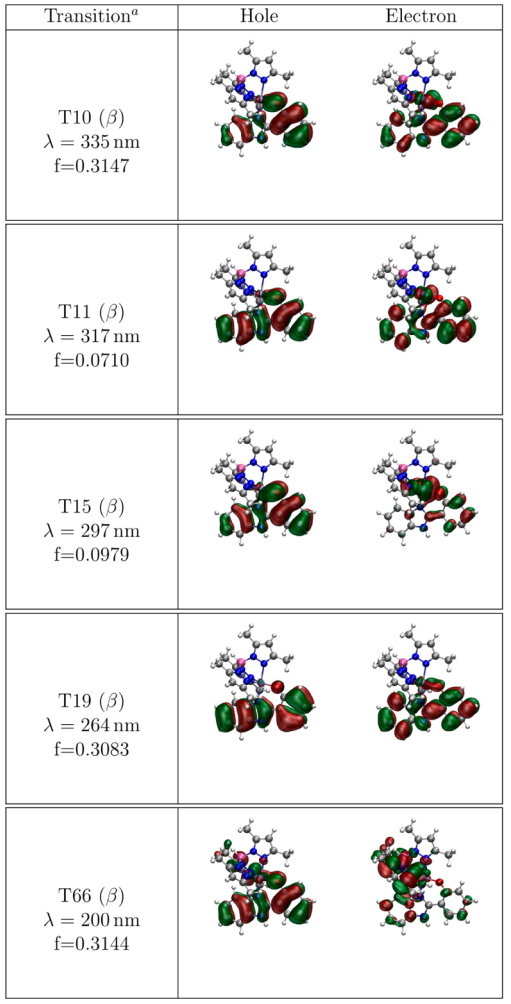

Figure 9. Selected NTO plots representing hole → electron transitions of complex **1** calculated using the TD-CAM-B3LYP method in $CHCl_3$ solution.

From here on, the density of electronic states noticeably increases with energy and accordingly the number of electronic transitions also increases, as observed in the simulated spectrum of the complex **1** depicted in the bottom of Figure 5. It thus becomes much more difficult to characterize the electronic transitions, especially by using the MO contributions whose weights rapidly scatter along the electronic wave functions. Nevertheless, by NTO analysis we find that the most intense transition to state 66 in this higher energy region is a ligand-to-ligand charge-transfer (LL′CT) transition, as shown in Figure 9. The superposition and convolution of the multitude of electronic transitions occurring in this high energy region now originate the absorption band of complex **1** peaked at 242 nm.

The electronic transitions of complex **2** follow a very similar pattern to that of complex **1**, as observed by comparing the corresponding simulated spectra shown in bottom panels of Figures 5 and 6. The most important features of the transitions are detailed in Table 3 and illustrated in the MO diagram of Supporting Information Figure S4. First, we have the lowest energy H → L transition to state 10, which is a charge transfer $\pi \rightarrow \pi^*$ transition within the benzoxazolate pbx ligand modified by the Ni ion and which gives rise to the absorption band observed at 374 nm. Next come the two less intense H(β) → L + 1(β) transitions to states 11 and 15 responsible for the weak absorption band observed at 338 nm, with a clear charge transfer occurring in the transition to state 15 from the pbx ligand to the metal clearly shown in Supporting Information Figure S4 and Table S2. The stronger transition to state 19 follows, in which the displacement of charge transfer occurs within the ligand, and which results in the experimental band that peaked at 293 nm. Finally, we have the congestion of transitions taking place at higher energies, which all merge to give the most intense band of the spectra around 240 nm. The most intense transition to state 70 occurs in this case within the Tp* ligand, as observed in Supporting Information Table S2.

As far as complex **3** containing the benzothiazolate pbt ligand is concerned, some variations are noticed in the simulated spectra (Figure 7, bottom). First we see that the two LMCT transitions to states 11 and 16 are significantly less intense than those in complexes **1** and **2**, providing an explanation for the extreme weakness of the experimental band at 343 nm, and second, the absorption band observed at 296 nm rises now from two ILCT transitions to states 19 and 23, instead of from a single one transition to state 19 as occurs in the other two complexes. In the crowded high-energy region, we can see now that the transition to the excited state 78 undergoes with substantial charge transfer from the Ni atom to the pbt ligand, as observed in Supporting Information Table S3.

dx.doi.org/10.1021/ic5001655 | Inorg. Chem. 2014, 53, 5502−5514

Luminescence Properties and Optical Response of Complexes 1−3 to Zn(II), Cd(II), Hg(II), and Cu(II). Complexes **1**−**3** are moderately blue luminescent at room temperature, both in chloroform solution and in solid state. The corresponding excitation and emission spectra are shown in Figures 10 (solution) and 11 (solid state), and the

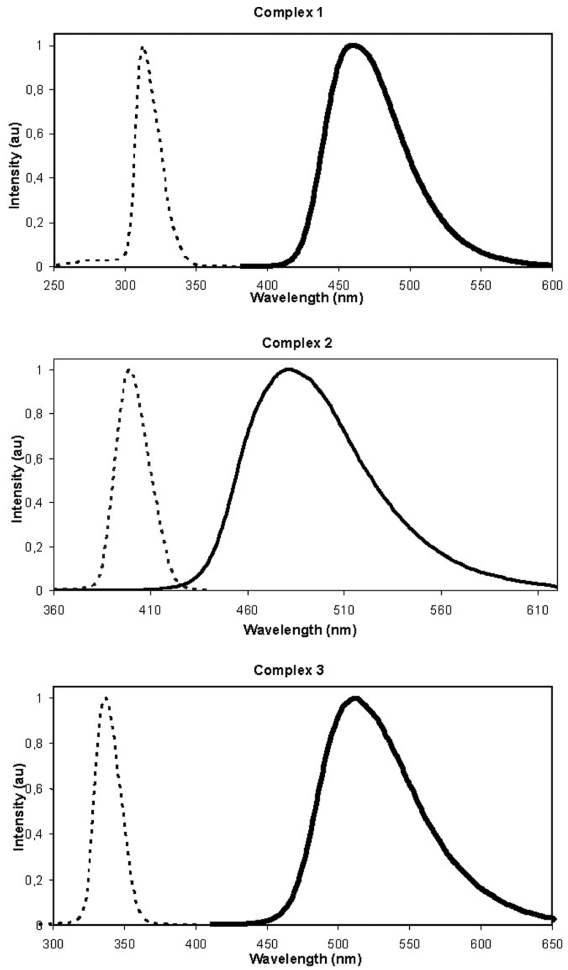

Figure 10. Emission (solid line) and excitation (dashed line) spectra from complexes **1**−**3** in chloroform solutions.

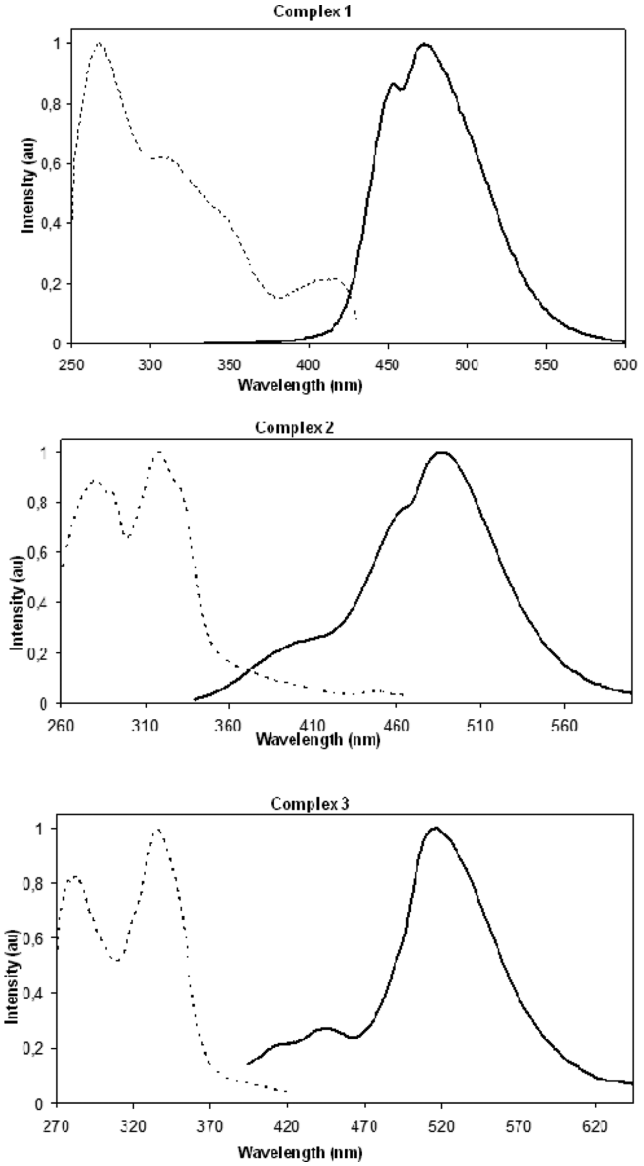

Figure 11. Emission (solid line) and excitation (dashed line) spectra from complexes **1**−**3** in solid state.

luminescence data are collected in Table 5. The quantum yields were measured and examined by comparative method using Coumarin-314 in ethanol as standard (Φ_{ST} = 0.68). We also include in Table 5 for comparison the excitation and emission wavelengths of the three ligands, Hpbm, Hpbx, and Hpbt, in dichloromethane solution recently reported by Jain et al.[46]

The luminescence of the three nickel complexes comes from the HOMO−LUMO transition which, as discussed above, is a $\pi \rightarrow \pi^*$ transition that occurs within the benzazolate ligand slightly assisted by the coordination metal. This transition is reminiscent of that taking place in the free ligands, Hpbm, Hpbx, or Hpbt, where the well-known photoinduced enol−keto tautomerization governs the luminescence spectra.[15,47] As shown in Figure 10, the emission spectra of the three complexes in chloroform display broad structureless bands at 460 (**1**), 482 (**2**), and 512 (**3**) nm. These bands should be, in principle, red-shifted with respect to the benzazolate bands due to coordination to the nickel metal. However, by comparing their emission wavelengths with those of the free ligands measured by Jain et al., which are 460 (Hpbm), 490 (Hpbx), and 528 (Hpbt) nm, we see that complex **1** shows no shift, and that the emission bands of complexes **2** and **3** are, respectively, blue-shifted in 8 and 16 nm with respect to those of the free ligands. This behavior is presumably due to deprotonation of the ligand to bind the nickel ion and the resulting suppression of the keto form in the excited state of the complex, which eliminates the possibility of intramolecular proton transfer that reduces the HOMO−LUMO gap.

The quantum efficiencies of the complexes, included in Table 5, reveal that the benzothiazole ligand increases considerably the luminescence of complex **3** (0.194) as compared to complexes **1** (0.027) and **2** (0.048) which contain the benzimidazole and benzoxazole ligands, respectively. Complex **3** turns out to be again, in this sense, somewhat different from **1** and **2**, as occurs with the absorption spectrum. Also, in the structure of **3**, the phenyl and benzazolate rings are at an angle of 1.80° almost flat, compared with **1** and **2** in which the corresponding angles are 5.22° and 11.24°, respectively.

dx.doi.org/10.1021/ic5001655 | Inorg. Chem. 2014, 53, 5502−5514

Table 5. Luminiescent Spectra Data for Complexes 1−3 in Chloroform Solution and Solid State

	solution					solid state			
	emission		excitation			emission		excitation	
compd	λ_{exc}	λ_{max}	λ_{em}	λ_{max}	ϕ^a	λ_{exc}	λ_{max}	λ_{em}	λ_{max}
1	312	460	462	313	0.027	312	453, 473	452	268, 310, 327, 347, 416
2	320	482	480	319	0.048	320	398, 461, 486	485	280, 290, 318, 330
3	336	512	512	337	0.194	336	420, 446, 516	515	284, 335
Hpbm[b]	353	460							
Hpbx[b]	354	490							
Hpbt[b]	375	528							

[a]Coumarin-314 in ethanol as standard, Φ_{ST} = 0.68. [b]Ref 46.

The observed emissions of the complexes in the solid state, at room temperature, are not significantly different from emission in solution (Figure 11), except for the fact that the complexes show now structured bands at λ_{max} 473, 486, and 516 nm which are likely due to the different structural arrangements of the benzazolate ligands.

Apart from affecting the electronic properties of the three complexes, the benzazole ligands with different donor heteroatoms in the benzazole ring might result in the complexes acting as probes for recognition of M(II) cations. Accordingly, to obtain an approach to the fluorescent response of **1**−**3** to metal ions, we have investigated the changes of their fluorescence properties by screening for responses to cations Zn(II), Cd(II), Hg(II), and Cu(II), each in 2 equiv excess. Figures 12 and 13 and Supporting Information Figure S6 show

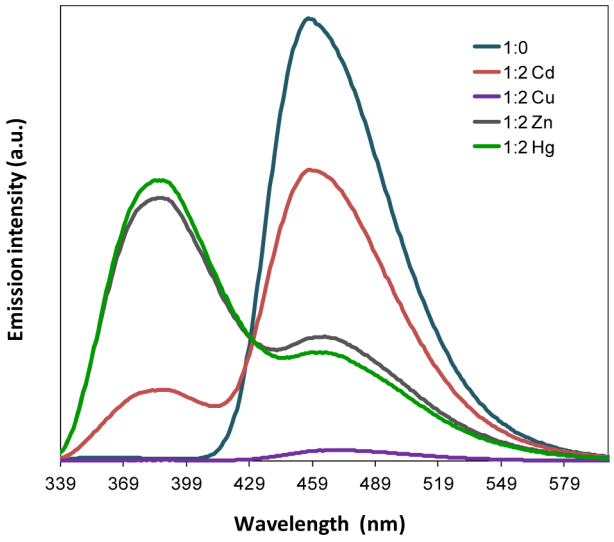

Figure 12. Fluorescence response of complex **2** (10^{-5} M at 20 °C) in $CHCl_3$/iPrOH (1:2) solution upon addition of 2 equiv metal ions as aqueous solutions of $Zn(ClO_4)_2{\cdot}6H_2O$, $Cd(ClO_4)_2{\cdot}6H_2O$, $Hg(CF_3SO_3)_2$, and $CuSO_4$.

the fluorescent responses of the complexes ($CHCl_3$/*i*PrOH, 1:2, 10^{-5} M at 20 °C) to the metal ions in aqueous solutions which, as observed, are noticeably different. In complex **1**, the emission intensity decreases in the presence of Zn(II), Hg(II), and Cu(II) (Supporting Information Figure S6), but undergoes no substantial change when Cd(II) is added. In complex **2** (Figure 12), the emission intensity also decreases upon addition of Zn(II), Cd(II), and Hg(II), although accompanied now by the appearance of a new band at ∼380 nm. The most noticeable finding in this case is, however, the strong intensity

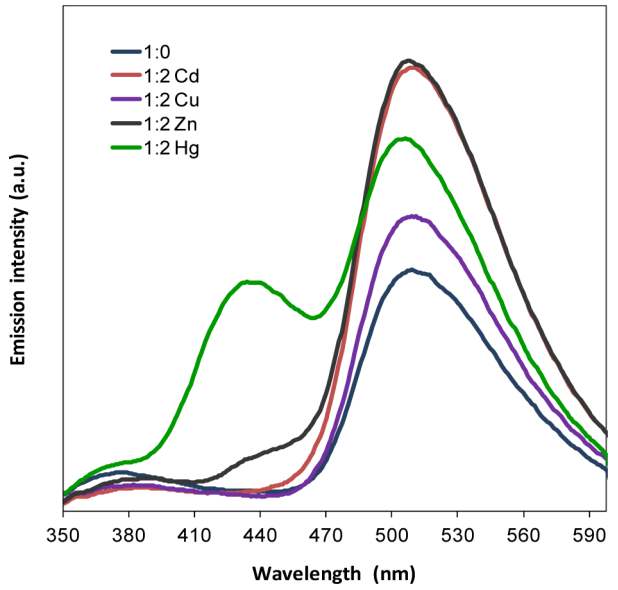

Figure 13. Fluorescence response of complex **3** (10^{-5} M at 20 °C) in $CHCl_3$/iPrOH (1:2) solution upon addition of 2 equiv metal ions as aqueous solutions of $Zn(ClO_4)_2{\cdot}6H_2O$, $Cd(ClO_4)_2{\cdot}6H_2O$, $Hg(CF_3SO_3)_2$, and $CuSO_4$.

quenching that occurs in the presence of Cu(II), which opens the possibility of using complex **2** as a turn-off molecular probe toward Cu(II). As for complex **3**, the fluorescence emission, on the contrary, enhances in the presence of the four cations Zn(II), Cd(II), Hg(II), and Cu(II) (Figure 13), with a new band appearing only for Hg(II) at about 430 nm.

We have also studied the variation of the luminescence intensity of the complexes with rising concentrations of the cations Zn(II), Cd(II), Hg(II), and Cu(II). The most significant changes occur in complexes **2** and **3**. In particular, for complex **2** we clearly observe the quenching of the emission at 450 nm upon addition of Cu(II) in amounts from 0.2 to 50 equiv (Figure 14), as well as the appearance of the new emission band at 390 nm as the luminescence intensity at 465 nm decreases when Zn(II) (0.2−50 equiv) is added (Supporting Information Figure S7). The addition of Cd(II) (0.2−50 equiv) to a solution of complex **2** causes the same effect, although the increase in the emission intensity at 390 nm is not as great as that caused by the addition of Zn(II) (Supporting Information Figure S8). A similar behavior is observed when Hg(II) is added to the solution of complex **2** (not shown).

It is therefore clear that the intensity of the ILMMCT transition responsible for the fluorescence of the complexes is

dx.doi.org/10.1021/ic5001655 | *Inorg. Chem.* 2014, 53, 5502−5514

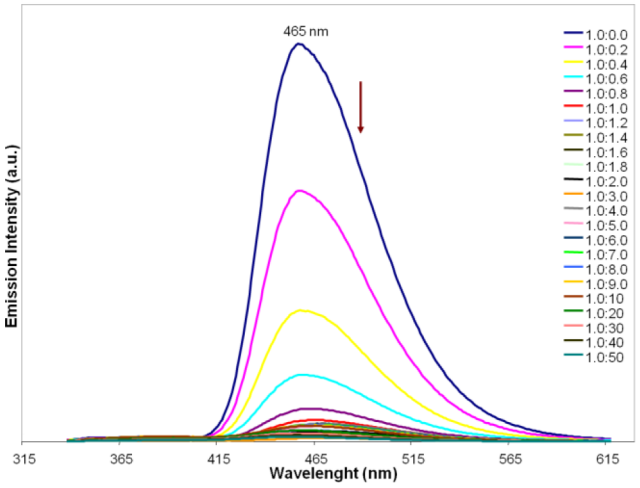

Figure 14. Fluorescence spectra upon addition of Cu(II) ion (0.0−50 equiv) to a solution of **2** (10^{-5} M) in $CHCl_3$/iPrOH (1:2).

rather dependent on the interaction with the M(II) cations. In complex **2**, these cations apparently interact with the oxygen atom of the benzoxazole and modify the electronic density of the ring in such a way that the charge transfer within the ligand reduces whereas the charge transfer from the ligand to the metal increases, thus explaining the luminescence drop at 460 nm. The emergence of the new emission band at 390 nm is likely due to a second electronic transfer mechanism from ligand to metal.

The variation of the luminescence intensity of complex **3** upon addition of different amounts of the M(II) cations is different from that of complex **2**. As discussed above, the luminescence is now enhancing instead of diminishing, as clearly shown in Supporting Ifnformation Figure S9 depicting the increase of the luminescent intensity of complex **3** at 510 nm upon addition of Cd(II) (0−15 equiv). A similar increase of the emission intensity at 510 nm is observed when Zn(II) (0−50 equiv) is added, with the appearance now of two new emission bands at 445 and 380 nm (Figure 15). However, the most significant changes occur upon addition of Hg(II) (0−100 equiv), which again originates two new emission bands at 436 and 380 nm although they are much more intense than those resulting from Zn(II) addition (Supporting Information Figure S10). In complex **3**, the sulfur atom of the benzothiazole ring may interact with the cations M(II) favoring the internal charge transfer within the ligand and also increasing the charge transfer from the metal to ligand. The first effect may justify an increase in intensity at 510 nm, and the second mechanism would explain the emergence of new higher energy emission bands.

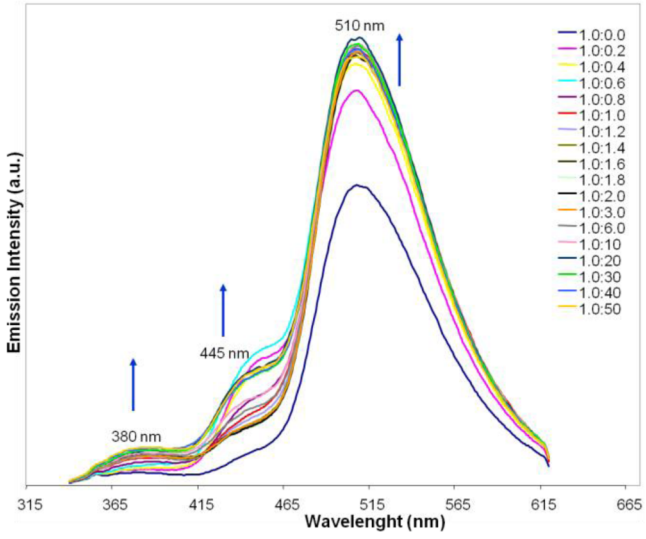

Figure 15. Fluorescence spectra upon addition of Zn(II) ion (0.0−50 equiv) to a solution of **3** (10^{-5} M) in $CHCl_3$/iPrOH (1:2).

To summarize, while the addition of cations Zn(II), Cd(II), Hg(II), and Cu(II) to complexes **1** and **2** results in a decrease in luminescent intensity, adding these cations to the complex **3** solution leads to an increase in intensity. Hence, complexes containing different donor atoms in the corresponding benzazole ligand give different luminescence responses in the presence of metal ions. Complexes **1** and **2**, which have σ-donor atoms such as N and O, decrease luminescent intensity in the presence of Zn(II), Cd(II), Hg(II), and Cu(II), and complex **3**, instead, containing the π- acceptor S presents enhanced luminescence response.

CONCLUSIONS

Pentacoordinate Ni(II) complexes containing benzazole type ligands and Tp* (hydrotris(3,5-dimethylpyrazolyl)borate) have been prepared via acid−base reactions using $[Ni(Tp^*)(\mu\text{-}OH)]_2$ as precursor. The structures of all complexes have been established by X-ray crystallography. The ^1H NMR spectra of the complexes present sharp isotropically shifted signals. $\{^1H-^1H\}$-COSY spectra were used for assigning all resonances. The resonance lines pattern observed for the benzazole ligands was indicative of two mechanism of spin delocalization. DFT calculations were used to optimize the structures of the three complexes. The UV−vis spectra were simulated in chloroform by TD-DFT and reproduce the main features of the experimental spectra. The simulated spectra showed that the LMCT transition became weaker from complex **1** to complexes **2** and **3**, which gave an explanation for the experimental band at 343 nm. In the high-energy region, a substantial charge transfer from the Ni atom to the pbt ligand is proposed in complex **3**. Complexes **1**−**3** are moderately blue luminescent at room temperature, both in the solid state and in solution. The emissions could be attributed predominantly to a ligand-centered (LC) excited state, although a mixed nature with contribution from Ni(II) atoms is also possible. The quantum efficiencies were 0.027 for complex **1**, 0.048 for **2**, and 0.194 for **3**, with the benzothiazole ligand increasing, as observed, considerably the luminescence compared to benzimidazole and benzoxazole derivatives. The changes in fluorescence properties of complexes toward ions Zn(II), Cd(II), Hg(II), and Cu(II) have been established. The addition of these cations to complexes **1** and **2** resulted in a decrease in luminescent intensity, and adding them to the complex **3** solution led to an increase in intensity. In summary, the pentacoordinate Ni(II) complexes containing benzazole type ligands studied in this work show a luminescent response toward metal ions that can be modulated by the donor atom present in the corresponding benzazole ligand. More studies to generalize these observations are currently in progress.

EXPERIMENTAL SECTION

General Methods. Infrared spectra were recorded on a PerkinElmer 16F PC FT-IR spectrophotometer using Nujol mulls between polyethylene sheets. Accurate mass measurements were

dx.doi.org/10.1021/ic5001655 | Inorg. Chem. 2014, 53, 5502−5514

performed on an Agilent 6220 time-of-flight MS coupled to a HPLC Agilent series 1200 and equipped with an ionization source electrospray-APCI. The instrument was operated in the positive ion mode using a mass range 25−20 000 m/z. C, H, N, and S analyses were performed with a Carlo Erba model EA 1108 microanalyzer. ^{1}H NMR spectra were recorded on Bruker spectrometers (AC 200E or AC 400E) using $SiMe_4$ as standard. The $\{^1H-^1H\}$ COSY spectrum was recorded on a Bruker 200 MHz spectrometer at 20 °C in $CDCl_3$ solution with 512 data points in the F1 dimension and 1024 data points in the F2 dimension with a delay time of 500 ms for **1** and 9 ms for **2** and **3**, respectively. Experimental parameters were varied to obtain the best resolution and the signal-to-noise. The UV−vis spectra (in chloroform) were recorded on a UNICAM UV 500 spectrophotometer for 250−800 nm range. Excitation and emission spectra were recorded on a Jobin Yvon Fluorolog 3-22 spectrofluorometer with a 450 W xenon lamp, double-grating monochromators, and a TBX-04 photomultiplier. The solution measurements were carried out in a right angle configuration using degassed solutions of the samples in 10 mm quartz fluorescence. The solid-state emission spectra of the complexes were recorded by placing a uniform layer of powder between two quartz plates.

Materials. All of the chemicals were purchased from Aldrich and were used without further purification. Solvents were dried and distilled by general methods before use. The complex $[Ni(Tp^*)(\mu\text{-}OH)]_2$ (Tp* = hydrotris(3,5-dimethylpyrazolyl)borate) was prepared by previously described procedures.[37] Solvents were dried and distilled by general methods before use.

Synthesis of [Ni(Tp*)(pbz)]. Complexes **1**−**3** were prepared by reaction of $[NiTp^*(\mu\text{-}OH)]_2$ (0.134 mmol) with the corresponding benzazole (0.268 mmol) [Hpbm = 2-(2′-hydroxylphenyl)-benzimidazole, Hpbx = 2-(2′-hydroxylphenyl)benzoxazole, and Hpbt = 2-(2′-hydroxylphenyl)benzothiazole], in chloroform (50 mL). After stirring for 24 h the solution was evaporated under reduced pressured, and *n*-hexane was added to the solution. The resulting green solid was collected by filtration, washed with *n*-hexane, and air-dried.

[Ni(Tp)(pbm)] (1).* The yield was 144.9 mg, green (96%). Anal. Calcd (%) for $C_{28}H_{31}BN_8NiO$ (565.13): C 59.51; H 5.53; N 19.83. Found: C 58.85; H 5.58; N 19.09. TOF-MS (m/z): 565.2151 [M]; IR (nujol): 3325 (ν_{NH}), 2511 (ν_{BH}), 1623, 1607 ($\nu_{C=C}$), 1548 ($\nu_{C=N}$), 1526 ($\nu_{C=N}$) cm^{-1}. ^{1}H NMR (400 MHz; $CDCl_3$): 65.42 (4-H_{ax}-Tp*, 1H), 61.75 (4-H_{eq}-Tp*, 2H), 32.18 (H_7, 1H), 29.96 (H_8, 1H), 13.57 (H_6, 1H), 8.83 (H_5, 1H), 5.32 (H_4, 1H), 3.25 (H_3, 1H), 1.58 (5-Me_{eq}-Tp*, 6H), −2.98 (H_2, 1H), −3.47 (5-Me_{ax}-Tp*, 3H), −6.39 (H_1, 1H), −7.11 (3-Me_{ax}-Tp*, 3H), −9.80 (3-Me_{eq}-Tp*, 6H), −13.42 (HB-Tp*) ppm.

[Ni(Tp)(pbx)] (2).* The yield was 110.3 mg, green (73%). Anal. Calcd (%) for $C_{28}H_{30}BN_7NiO_2$ (566.11): C 59.41; H 5.34; N 17.32. Found: C 58.92; H 5.27; N 17.06. TOF-MS (m/z): 566.1973 [M]. IR (nujol): 2511 (ν_{BH}), 1617 ($\nu_{C=C}$), 1559 ($\nu_{C=N}$), 1543 ($\nu_{C=N}$) cm^{-1}. ^{1}H NMR (400 MHz; $CDCl_3$): 67.07 (4-H_{ax}-Tp*, 1H), 63.61 (4-H_{eq}-Tp*, 2H), 32.37 (H_7, 1H), 31.02 (H_8, 1H), 16.72 (H_6, 1H), 8.32 (H_5, 1H), 4.81 (H_4, 1H), 3.23 (H_3, 1H), 1.55 (5-Me_{eq}-Tp*, 6H), −3.83 (5-Me_{ax}-Tp*, 3H), −6.99 (H_2, 1H), −7.22 (3-Me_{ax}-Tp*, 3H), −9.06 (H_1, 1H), −9.85 (3-Me_{eq}-Tp*, 6H), −13.90 (HB-Tp*) ppm.

[Ni(Tp)(pbt)] (3).* The yield was 146.1 mg, green (94%). Anal. Calcd (%) for $C_{28}H_{30}BN_7NiOS$ (582.17): C 57.77; H 5.19; N 16.80; S 5.51. Found: C 57.50; H 5.15; N 16.84; S 4.94. TOF-MS (m/z): 582.1757 [M]. IR (nujol): 2513 (ν_{BH}), 1604 ($\nu_{C=C}$), 1545 ($\nu_{C=N}$), 1494 ($\nu_{C=N}$) cm^{-1}. ^{1}H NMR (400 MHz; $CDCl_3$): 68.01 (4-H_{ax}-Tp*, 1H), 62.71 (4-H_{eq}-Tp*, 2H), 28.17 (H_7, 1H), 27.25 (H_8, 1H), 10.66 (H_6, 1H), 9.33 (H_5, 1H), 5.30 (H_4, 1H), 3.39 (H_3, 1H), 1.45 (5-Me_{eq}-Tp*, 6H), −1.05 (H_2, 1H), −2.96 (5-Me_{ax}-Tp*, 3H), −5.81 (H_1, 1H), −7.77 (3-Me_{ax}-Tp*, 3H), −9.96 (3-Me_{eq}-Tp*, 6H), −13.35 (HB-Tp*) ppm.

Computational Details. The theoretical study of the three nickel complexes was carried out using DFT and TD-DFT methods, as implemented in the GAUSSIAN-09 program package.[48] After considering different density functionals and bases, the geometries of the triplet electronic ground states of the complexes were eventually optimized *in vacuo*, starting from the X-ray structures, by using the BP86 density functional[49] and a combination of the LANL2DTZ+ basis[50] for nickel and the cc-pVDZ basis[51] for the rest of the atoms. To simulate the absorption electronic spectra we used the TD-CAM-B3LYP method, which is properly suited (designed) to describe charge transfer transitions.[52] These calculations were carried out in chloroform solution using the polarizable continuum model with the integral equation formalism (IEF-PCM).[53] The first 100 triplet excited electronic states were computed covering transition energies of up to about 6.8 eV, and the spectral lines were widened using Gaussian functions with a width of 0.25 eV. The transitions to the electronic excited states were investigated by analyzing the canonical molecular orbitals (MO) and also the natural transitions orbitals (NTOs),[54] which provide the best representation of the electronic excitations in terms of single particles.

■ ASSOCIATED CONTENT

Ⓢ Supporting Information

^{1}H NMR spectra of complexes **1** and **2**; $\{^1H-^1H\}$ COSY of complex **3**; molecular orbital energy diagrams of **2** and **3**, and NTO plots for the main electronic transitions of **1**, **2**, and **3**, from TD-DFT calculations. Fluorescence response of complexes **1**, **2**, and **3** upon addition metal ions. Crystallographic data in CIF format. This material is available free of charge via the Internet at http://pubs.acs.org."

■ AUTHOR INFORMATION

Corresponding Authors

*E-mail: dsl@um.es. Phone: +34 868 887458. Fax: +34 868 884148.

*E-mail: zuniga@um.es. Phone: +34 868 887439. Fax: +34 868 884148.

Notes

The authors declare no competing financial interest.

■ ACKNOWLEDGMENTS

This work was partially supported by the Spanish Ministerio de Ciencia e Innovación under Projects CTQ2011-25972 and CONSOLIDER CSD2009-00038, and by the Fundación Séneca del Centro de Coordinación de la Investigación de la Región de Murcia under Projects 08735/PI/08 and 08670/PI/08. J.C. acknowledges a FPU fellowship provided by the Ministerio de Educación of Spain.

■ REFERENCES

(1) For selected examples, see: (a) Tang, C. W.; VanSlyke, S. A. *Appl. Phys. Lett.* **1987**, *51*, 913−915. (b) Chen, C. H.; Shi, J. *Coord. Chem. Rev.* **1998**, *171*, 161−174. (c) Brinkmann, M.; Gadret, G.; Muccini, M.; Taliani, C.; Masciocchi, N.; Sironi, A. *J. Am. Chem. Soc.* **2000**, *122*, 5147−5157. (d) Kulkarni, A. P.; Tonzola, C. J.; Babel, A.; Jenekhe, S. A. *Chem. Mater.* **2004**, *16*, 4556−4573. (e) Pérez-Bolívar, C.; Takizawa, S.; Nishimura, G.; Montes, V. A.; Anzenbacher, P., Jr. *Chem.—Eur. J.* **2011**, *17*, 9076−9082.

(2) Sakio, S.; Miyaoka, S.; Kaneko, S., Fujii, T.; Takai, T. Japan Patent 2,001,125,292, 2001.

(3) Sato, Y. Japan Patent 6,336,586, 1994.

(4) Shi, S. Q. Taiwan Patent 401,453, 2000.

(5) (a) Nakamura, N.; Miyairi, K. European Patent 0,801,518, 1997. (b) Nakamura, N.; Wakabayashi, S. European Patent 0,652,273, 1995.

(6) Henary, M. M.; Fahrni, C. J. *J. Phys. Chem. A* **2002**, *106*, 5210−5220.

(7) Santra, S.; Krishnamoorthy, G.; Dogra, S. K. *J. Mol. Struct.* **2001**, *559*, 25−39.

(8) Moeller, M. G.; Campo, L. F.; Brandelli, A.; Stefani, V. *J. Photochem. Photobiol., A* **2002**, *149*, 217−225.

(9) Wang, K.; Huang, L.; Gao, L.; Huang, C.; Jin, L. *Solid State Commun.* **2002**, *122*, 233−236.

(10) Grevy, J. M.; Tellez, F.; Bernés, S.; Nöth, H.; Contreras, R.; Barba-Behrens, N. *Inorg. Chim. Acta* **2002**, *339*, 532−542.
(11) Bharti, N.; Maurya, M. R.; Naqvi, F.; Azam, A. *Bioorg. Med. Chem. Lett.* **2000**, *10*, 2243−2245.
(12) Ceniceros-Gómez, A. E.; Barba-Behrens, N.; Bernés, S.; Nöth, H.; Castillo-Blum, S. E. *Inorg. Chim. Acta* **2000**, *304*, 230−236.
(13) Castillo-Blum, S. E.; Barba-Behrens, N. *Coord. Chem. Rev.* **2000**, *196*, 3−30.
(14) Vourloumis, D.; Takahashi, M.; Simonsen, K. B.; Ayida, B. K.; Barluenga, S.; Winters, G. C.; Hermann, T. *Tetrahedron Lett.* **2003**, *44*, 2807−2811.
(15) Kwon, J. E.; Park, S. Y. *Adv. Mater.* **2011**, *23*, 3615−3642.
(16) Zhao, J.; Ji, S.; Chen, Y.; Guo, H.; Yang, P. *Phys. Chem. Chem. Phys.* **2012**, *14*, 8803−8817.
(17) (a) Williams, D. L.; Heller, A. *J. Phys. Chem.* **1970**, *74*, 4473−4480. (b) Nagaoka, S.; Kusunoki, J.; Fujibuchi, T.; Hatakenaka, S.; Mukai, K.; Nagashima, U. *J. Photochem. Photobiol., A* **1999**, *122*, 151−159.
(18) Costela, A.; Amat, F.; Catalán, J.; Douhal, A.; Figuera, J. M.; Muñoz, J. M.; Acuña, A. U. *Opt. Commun.* **1987**, *64*, 457−460.
(19) (a) Tarkka, R. M.; Zhang, X.; Jenekhe, S. A. *J. Am. Chem. Soc.* **1996**, *118*, 9438−9439. (b) Liang, F.; Wang, L.; Ma, D.; Jing, X.; Wang, F. *Appl. Phys. Lett.* **2002**, *81*, 4−6. (c) Kimand, S.; Park, S. Y. *Adv. Mater.* **2003**, *15*, 1341−1344. (d) Kang, J.-W.; Kim, S.; Park, S. Y.; Kim, J.-J. *Appl. Phys. Lett.* **2004**, *84*, 4221−4223.
(20) Sakai, K.; Tsuzuki, T.; Itoh, Y.; Ichikawa, M.; Taniguchi, Y. *Appl. Phys. Lett.* **2005**, *86*, 081103.
(21) Tong, Y.-P.; Zheng, S.-L.; Chen, X.-M. *Inorg. Chem.* **2005**, *44*, 4270−4275.
(22) Henary, M. M.; Fahrni, C. J. *J. Phys. Chem. A* **2002**, *106*, 5210−5220.
(23) (a) Rodembusch, F. S.; Brand, F. R.; Correa, D. S.; Pocos, J. C.; Martinelli, M.; Stefani, V. *Mater. Chem. Phys.* **2005**, *92*, 389−393. (b) Jang, Y. K.; Kim, D. E.; Kim, W. S.; Kim, B. S.; Kwan, O. K.; Lee, B. J.; Kwon, Y. S. *Thin Solid Films* **2007**, *515*, 5075−5078. (c) Ouezada-Buendia, X.; Esparza-Ruiz, A.; Pena-Hueso, A.; Barba-Behrens, N.; Contreras, R.; Flores-Parra, A.; Bernes, S.; Castillo-Blum, S. E. *Inorg. Chim. Acta* **2008**, *361*, 2759−2767.
(24) Li, H.; Wu, Y.-J.; Xu, C.; Tian, R.-Q. *Polyhedron* **2007**, *26*, 4389−4396.
(25) (a) Sykora, J.; Sima, J. *Photochemistry of Coordination Compounds*; Veda: Amsterdam, 1990. (b) Balzani, V.; Scandola, F. *Supramolecular Photochemistry*; Springer: Chichester, U.K.,1991.
(26) de Silva, A. P.; Gunaratne, H. Q. N.; Gunnlaugsson, T.; Huxley, A. J. M.; McCoy, C. P.; Rademacher, J. T.; Rice, T. E. *Chem. Rev.* **1997**, *97*, 1515−1566.
(27) Shavaleev, N. M.; Adams, H.; Best, J.; Edge, R.; Navaratnam, S.; Weinstein, J. A. *Inorg. Chem.* **2006**, *45*, 9410−9415.
(28) Ghedini, M.; Aiello, I.; La Deda, M.; Grisolia, A. *Chem. Commun.* **2003**, 2198−2199.
(29) (a) Van Houten, K. A.; Heath, D. C.; Barringer, C. A.; Rheingold, A. L.; Pilato, R. S. *Inorg. Chem.* **1998**, *37*, 4647−4653. (b) Barigelletti, F.; Sandrini, D.; Maestri, M.; Balzani, V.; Vonzelewsky, A.; Chassot, L.; Jolliet, P.; Maeder, U. *Inorg. Chem.* **1988**, *27*, 3644−3647. (c) Wu, Q. G.; Hook, A.; Wang, S. N. *Angew. Chem., Int. Ed.* **2000**, *39*, 3933−3935. (d) Song, D. T.; Wu, Q. G.; Hook, A.; Kozin, I.; Wang, S. N. *Organometallics* **2001**, *20*, 4683−4689.
(30) (a) Zhang, Z.-Q.; Huang, R.-D.; Dong, L.-J.; Xu, Y.-Q.; Yu, L.-Q.; Jiao, Z.-W.; Hu, C.-W. *Inorg. Chim. Acta* **2009**, *362*, 3056−3064. (b) Naskar, S.; Naskar, S.; Butcher, R. J.; Chattopadhyay, S. K. *Inorg. Chim. Acta* **2010**, *363*, 3641−3646. (c) Dalai, S.; Rana, A.; Bera, M.; Chowdhuri, D. S.; Zangrando, E. *Inorg. Chim. Acta* **2010**, *363*, 1843−1848. (d) Schnuriger, M.; Tague, E.; Richter, M. M. *Inorg. Chim. Acta* **2011**, *379*, 158−162. (e) Santana, M. D.; García-Bueno, R.; García, G.; Pérez, J.; García, L.; Monge, M.; Laguna, A. *Dalton Trans.* **2010**, *39*, 1797−1806. (f) Xu, J.-Y.; Xie, C.-Z.; Xue, F.; Hao, L.-F.; Ma, Z.-Y.; Liao, D.-Z.; Yan, S.-P. *Dalton Trans.* **2010**, *39*, 7159−7166. (g) Barwiolek, M.; Szlyk, E.; Muzioł, T. M.; Lis, T. *Dalton Trans.* **2011**, *40*, 11012−11022. (h) Bhattacharjee, C. R.; Das, G.; Mondal, P. *Eur. J. Inorg. Chem.* **2011**, 5390−5396.
(31) (a) Machura, B.; Wolf, M.; Palion, J.; Switlicka, A.; Nawro, I.; Michalik, K. *Struct. Chem.* **2011**, *22*, 1053−1064. (b) Pilia, L.; Espa, D.; Barsella, A.; Fort, A.; Makedonas, C.; Marchio, L.; Mercuri, M. L.; Serpe, A.; Mitsopoulou, A.; Deplano, P. *Inorg. Chem.* **2011**, *50*, 10005−10027. (c) Xiong, J.; Li, G.-N.; Sun, L.; Li, Y.-Z.; Zuo, J.-L.; You, X.-Z. *Eur. J. Inorg. Chem.* **2011**, 5173−5181. (d) Huang, D.; Makhlynets, O. V.; Tan, L. L.; Lee, S. C.; Rybak-Akimova, E. V.; Holm, R. H. . *Inorg. Chem.* **2011**, *50*, 10070−10081. (e) Coxtes, J.-P.; Maurice, R.; Vendier, L. *Chem.—Eur. J.* **2012**, 4031−4040. (f) Ruamps, R.; Maurice, R.; Batchelor, L.; Boggio-Pasqua, M.; Guillot, R.; Barra, A. L.; Liu, J.; Bendeif, E.-E.; Pillet, S.; Hill, S.; Mallah, T.; Guihery, N. *J. Am. Chem. Soc.* **2013**, *135*, 3017−3026.
(32) (a) Cao, L. Y.; Jennings, M. C.; Puddephatt, R. J. *Dalton Trans.* **2009**, 5171−5176. (b) Ortiz, A. L.; Cumbrera, F. L.; Pérez, J.; Meléndez-Martínez, J. J.; Palatinus, L. *J. Alloys Compd.* **2009**, *467*, 322−322. (c) Adrian, R. A.; Broker, G. A.; Tiekink, E. R. T.; Walmsley, J. A. *Inorg. Chim. Acta* **2008**, *361*, 1261−1266. (d) Adrian, R. A.; Zhu, S.; Powell, D. R.; Broker, G. A.; Tiekink, E. R. T.; Walmsley, J. A. *Dalton Trans.* **2007**, 4399−4404. (e) Roesky, H. W.; Singh, S.; Yusuff, K. K. M.; Maguire, J. A.; Hosmane, N. S. *Chem. Rev.* **2006**, *106*, 3813−3843 and references therein. (f) Sodeoka, M.; Hamashima, Y. *Pure Appl. Chem.* **2006**, *78*, 477−494. (g) Yang, G. S.; Miao, R.; Li, I. Z.; Hong, J.; Zhao, S. M.; Guo, Z. J.; Zhu, L. G. *Dalton Trans.* **2005**, 1613−1619. (h) Kannan, S.; James, A. J.; Sharp, P. R. *Inorg. Chim. Acta* **2003**, *345*, 8−14. (i) Gilge, J. W.; Roesky, H. W. *Chem. Rev.* **1994**, *94*, 895−910.
(33) (a) Martin, J. W. L.; Johnston, J. H.; Curtis, N. F. *J. Chem. Soc., Dalton Trans.* **1978**, 68−76. (b) Escuer, A.; Vicente, R.; Ribas, J. *Polyhedron* **1992**, *11*, 453−456.
(34) (a) Santana, M. D.; García, G.; Pérez, J.; Molins, E.; López, G. *Inorg. Chem.* **2001**, *40*, 5701−5703. (b) Santana, M. D.; García, G.; Navarro, C. M.; Lozano, A. A.; Pérez, J.; García, L.; López, G. *Polyhedron* **2002**, *21*, 1935−1942. (c) Santana, M. D.; García, G.; Lozano, A. A.; López, G.; Tudela, J.; Pérez, J.; García, L.; Lezama, L.; Rojo, T. *Chem.—Eur. J.* **2004**, *10*, 1738−1746. (d) Santana, M. D.; Lozano, A. A.; García, G.; López, G.; Pérez, J. *Dalton Trans.* **2005**, *1*, 104−109. (e) Ruiz, J.; Santana, M. D.; Lozano, A.; Vicente, C.; García, G.; López, G.; Pérez, J.; García, L. *Eur. J. Inorg. Chem.* **2005**, 3049−3059. (f) Lozano, A. A.; Sáez, M.; Pérez, J.; García, L.; Lezama, L.; Rojo, T.; López, G.; García, G.; Santana, M. D. *Dalton Trans.* **2006**, 3906−3911. (g) García-Bueno, R.; Santana, M. D.; Sánchez, G.; García, J.; García, G.; Pérez, J.; García, L. *Dalton Trans.* **2010**, *39*, 5728−5736.
(35) Trofimenko, S. *Chem. Rev.* **1993**, *93*, 943−980.
(36) (a) Trofimenko, S. *Polyhedron* **2004**, *23*, 197−203. (b) Kolotilov, S. V.; Addison, A. W.; Trofimenko, S.; Dougherty, W.; Pavlishchuk, V. V. *Inorg. Chem. Commun.* **2004**, *7*, 485−488. (c) Pettinari, C. *Scorpionates II: Chelating Borate Ligands*; Imperial College Press: London, 2008. (d) Trofimenko, S. *Scorpionates: The Coordination Chemistry of Polypyrazolylborate Ligands*; Imperial College Press: London, 1999.
(37) (a) López-Banet, L.; Santana, M. D.; García, G.; García, L.; Pérez, J.; Rojo, T.; Lezama, L.; Costes, J.-P. *Inorg. Chem.* **2011**, *50*, 437−443. (b) Santana, M. D.; López-Banet, L.; García, G.; García, L.; Pérez, J.; Liu, M. *Eur. J. Inorg. Chem.* **2008**, 4012−4018. (c) López-Banet, L.; Santana, M. D.; García, G.; Pérez, J.; García, L.; Liu, M. *Polyhedron* **2012**, *31*, 575−586.
(38) (a) Hikichi, S.; Yoshizawa, M.; Sasakura, Y.; Komatsuzaki, H.; Moro-oka, Y.; Akita, M. *Chem.—Eur. J.* **2001**, *7*, 5011−5028. (b) Hikichi, S.; Tanaka, M.; Moro-oka, Y.; Kitajima, N. *J. Chem. Soc., Chem. Commun.* **1994**, 1737−1738.
(39) Addison, A. W.; Rao, T. N.; Reedijk, J.; Rijn, J. V.; Verschoor, G. C. *J. Chem. Soc., Dalton Trans.* **1984**, 1349−1356.
(40) Hammes, B. S.; Luo, X.; Chohan, B. S.; Carrano, M. W.; Carrano, C. J. *J. Chem. Soc., Dalton Trans.* **2002**, 3374−3380.

(41) Koch, W.; Holthausen, M. C. In *A Chemist's Guide to Density Funtional Theory*; Wiley-VCH Verlag GmbH: Weinheim, Germany, 2001.
(42) (a) Ram, M. S.; Riordan, C. G.; Ostrander, R.; Rheingold, A. L. *Inorg. Chem.* **1995**, *34*, 5884−5892. (b) Cho, J.; Yap, G. P. A.; Riordan, C. G. *Inorg. Chem.* **2007**, *46*, 11308−11315. (c) Chattopadhyay, S.; Deb, T.; Ma, H.; Petersen, J. L.; Young, V. G., Jr.; Jensen, M. P. *Inorg. Chem.* **2008**, *47*, 3384−3392.
(43) Chattopadhyay, S.; Deb, T.; Petersen, J. L.; Young, V. G., Jr.; Jensen, M. P. *Inorg. Chem.* **2010**, *49*, 457−467.
(44) Jaquemin, D.; Wathelet, V.; Perpete, E. A.; Adamo, C. *J. Chem. Theory Comput.* **2009**, *5*, 2420−2435.
(45) (a) Li, Z.; Badaeva, E.; Zhou, D.; Bjorgaard, J.; Glusac, K. D.; Killina, S.; Sun, W. *J. Phys. Chem. A* **2012**, *116*, 4878−4889. (b) Kornobis, K.; Ruud, K.; Kozlowski, P. M. *J. Phys. Chem. A* **2013**, *117*, 863−876. (c) Chantzis, A.; Very, T.; Monari, A.; Assfeld, X. *J. Chem. Theory Comput.* **2012**, *8*, 1536−1541.
(46) Pal, M. K.; Kushwah, N.; Manna, D.; Wadawale, A.; Sudarsan, V.; Ghanty, T. K.; Jain, V. K. *Organometallics* **2013**, *32*, 104−111.
(47) (a) Tong, Y. P.; Lin, Y. W. *Inorg. Chim. Acta* **2009**, *362*, 2033−2038. (b) Sakai, K.-i.; Takahashi, S.; Kobayashi, A.; Akutagawa, T.; Nakamura, T.; Dosen, M.; Kato, M.; Nagashima, U. *Dalton Trans.* **2010**, *39*, 1989−1995.
(48) Frisch, M. J.; Trucks, G. W.; Schlegel, H. B.; Scuseria, G. E.; Robb, M. A.; Cheeseman, J. R.; Scalmani, G.; Barone, V.; Mennucci, B.; Petersson, G. A.; Nakatsuji, H.; Caricato, M.; Li, X.; Hratchian, H. P.; Izmaylov, A. F; Bloino, J.; Zheng, G.; Sonnenberg, J. L.; Hada, M.; Ehara, M.; Toyota, K.; Fukuda, R.; Hasegawa, J.; Ishida, M.; Nakajima, T.; Honda, Y.; Kitao, O.; Nakai, H.; Vreven, T.; Montgomery, J. A., Jr.; Peralta, J. E.; Ogliaro, F.; Bearpark, M.; Heyd, J. J.; Brothers, E.; Kudin, K. N.; Staroverov, V. N.; Kobayashi, R.; Normand, J.; Raghavachari, K.; Rendell, A.; Burant, J. C.; Iyengar, S. S.; Tomasi, J.; Cossi, M.; Rega, N.; Millam, J. M.; Klene, M.; Knox, J. E.; Cross, J. B.; Bakken, V.; Adamo, C.; Jaramillo, J.; Gomperts, R.; Stratmann, R. E.; Yazyev, O.; Austin. A. J.; Cammi, R.; Pomelli, C.; Ochterski, J. W.; Martin, R. L.; Morokuma, K.; Zakrzewski, V. G.; Voth, G. A.; Salvador, P.; Dannenberg, J. J.; Dapprich, S.; Daniels, A. D.; Farkas, O.; Foresman, J. B.; Ortiz, J. V.; Cioslowski, J.; Fox, D. J.; *Gaussian 09 Revision A.2*; Gaussian Inc.: Wallingford, CT, 2009.
(49) (a) Becke, A. D. *Phys. Rev. A* **1988**, *38*, 3098−3100. (b) Perdew, J. P. *Phys. Rev. B* **1986**, *33*, 8822−8824.
(50) Roy, L. E.; Hay, P. J.; Martin, R. L. *J. Chem. Theory Comput.* **2008**, *4*, 1029−1031.
(51) (a) Dunning, J. T. H. *J. Chem. Phys.* **1989**, *90*, 1007−1023. (b) Davidson, E. R. *Chem. Phys. Lett.* **1996**, *260*, 514−518.
(52) Yanai, T.; Tew, D.; Handy, H. *Chem. Phys. Lett.* **2004**, *393*, 51−57.
(53) (a) Miertus, S.; Scrocco, E.; Tomasi. *J. Chem. Phys.* **1981**, *55*, 117−129. (b) Scalmani, G.; Frisch, M. J. *J. Chem. Phys.* **2010**, *132*, 114110.
(54) Martin, R. L. *J. Chem. Phys.* **2003**, *118*, 4775−4777.